


ORIGINAL ARTICLE

Open Access



Bone Milling: On Monitoring Cutting State and Force Using Sound Signals

Zhenzhi Ying¹, Liming Shu^{1,2*}  and Naohiko Sugita^{1,2}

Abstract

Efficient monitoring of bone milling conditions in orthopedic and neurosurgical surgery can prevent tissue, bone, and tool damage, and reduce surgery time. Current researches are mainly focused on recognizing the cutting state using force signal. However, the force signal during the milling process is difficult and expensive to acquire. In this study, a neural network-based method is proposed to recognize the cutting state and force during the bone milling process using sound signals. Numerical modeling of the cutting force is performed to capture the relationship between the cutting force and the depth of cut in the bone milling process. The force model is used to calibrate the training data to improve the recognition accuracy. Wavelet package transform is used for signal processing to understand bone-cutting phenomena using sound signals. The proposed system succeeds to monitor the bone milling process to reduce the surgical risk. Experiments on standard bone specimens and vertebrae also indicate that the proposed approach has considerable potential for use in computer-assisted and robot-assisted bone-cutting systems used in various types of surgery.

Keywords: Cutting state, Force, Milling, Artificial neural network

1 Introduction

Bone milling is an indispensable and technically demanding procedure in many orthopedic and neurosurgical operations. The bone as the “workpiece” in milling is mainly composed of two structures: cortical and cancellous bone layers. Surgeons tend to choose different cutting strategies in different bone layers because of the significantly different mechanical properties required to improve the efficiency of bone milling and thus reduce the burden on the patient. Moreover, surgeons must avoid nerve or tissue damage, which seriously affects postoperative recovery [1, 2]. For instance, lumbar laminectomy, which is known as one of the most challenging surgeries, requires removal of a portion of a vertebra called the lamina. To adjust the machining parameters and avoid damage on spinal cord during bone milling,

surgeons must determine the cutting state, i.e., the bone structure being cutting and extent of penetration of the cutting tool. Automatic detection and control in bone milling are essential to improving the safety of surgery and reducing the physical and mental fatigue of the surgeon [3, 4].

Adaptive control and monitoring of bone milling have attracted considerable interest in the development of computer- and robot-assisted technologies [5–7]. The purpose of monitoring the milling condition in surgery is to prevent tissue/bone/tool damage from the large cutting force and to optimize the machining parameters in different cutting states to reduce the surgery time [8]. One of the challenges in using an adaptive control or tool monitoring system is the accurate and real-time representation of the variation in machining variables, such as cutting force and state. Most current surgical computer-assisted and robot-assisted systems utilize computed tomography data-based image navigation systems and force sensors to track the real-time cutting state and force [7, 9, 10]. However, the two/three-dimensional marker

*Correspondence: l.shu@mfg.t.u-tokyo.ac.jp

¹ Department of Mechanical Engineering, School of Engineering, The University of Tokyo, 7-3-1 Hongo, Bunkyo-ku, Tokyo 1138656, Japan
Full list of author information is available at the end of the article

array needs to be manually fixed onto the bone based on the boney land marker for registration during surgery, which could introduce a random error of navigation that is not sufficient compared to the degree of precision required (< 1 mm) [11]. Additionally, the navigation and force sensor systems would significantly increase the cost and complexity of the surgical system.

Finding an effective and convenient monitoring method with a low cost is important for improving the performance and popularization of bone milling. Experienced surgeons can judge the cutting state of bone milling, optimize the machining parameters through sound signals, and perceive the cutting force through touch. Liao et al. [12] analyzed the difference in sound signals at various penetration depths and chip formations. They found that sound signals have considerable potential for use in monitoring bone milling. For the past few years, the rapid development in artificial neural network (ANN) provides a promising solution to the monitoring problems in machining of biological tissues [7, 13–15]. Kais et al. [10] developed ANN models to estimate the mean values of force and temperature in bone milling, which can be used as nonlinear constraint optimization functions. Dai et al. [16] integrated a sound signal with a single-layer neural network to determine the cutting state of a bone and found a predicted accuracy higher than 85%. Guan et al. [17] applied a sound signal to distinguish the cutting layer during bone drilling, and the recognition rate reached 84.2%. However, in previous studies, the prediction accuracy did not meet the high requirements of surgery. For bone milling, the axial depth of cut (ADOC) is an unknown quantity because of the complex structure of natural bone and is difficult to capture experimentally and in practice. An accurate label of the ADOC in the training dataset is an essential requirement in machine learning algorithms for bone milling monitoring. In addition, most previous studies only focused on the cutting state, but the cutting force is also an essential parameter in the adaptive control of bone milling.

In this study, we developed a cutting state and force monitoring system for laminectomy surgery using a sound signal with a neural network during vertebral lamina milling. A mechanistic model of the cortical and cancellous bone milling process was developed and verified experimentally and used to auto-label the training data in vertebra milling to improve the prediction accuracy of the monitoring system.

2 Bone Structure Analysis and Cutting Challenges in Vertebra Lamina Milling

The schematics of lumbar laminectomy and the anatomical structure of the vertebral lamina are shown in Figure 1. The vertebral lamina presents a sandwich structure

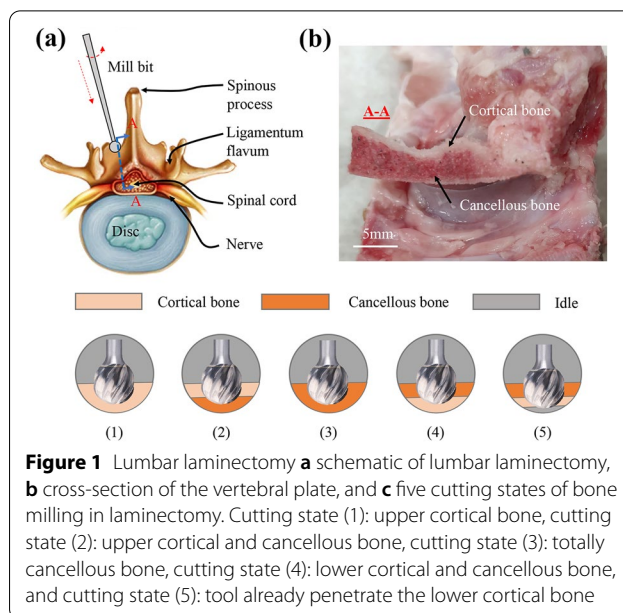


Figure 1 Lumbar laminectomy **a** schematic of lumbar laminectomy, **b** cross-section of the vertebral plate, and **c** five cutting states of bone milling in laminectomy. Cutting state (1): upper cortical bone, cutting state (2): upper cortical and cancellous bone, cutting state (3): totally cancellous bone, cutting state (4): lower cortical and cancellous bone, and cutting state (5): tool already penetrate the lower cortical bone

and is mainly composed of two different types of bone tissue: cortical and cancellous tissue. The cortical bone covers the surface of the vertebral plate and has a dense microscopic structure, whereas the cancellous bone is located inside the vertebral plate and is composed of a network-like tissue with porous spaces. This special bone structure makes the vertebral lamina capable of sustaining elevated mechanical loads with light weight. As shown in Figure 1b, the cross-section of the vertebral plate is irregular, with a slightly thicker side (3–5 mm), which may cause cutting challenges in vertebral lamina milling [18–20].

The strategy of vertebral lamina removal in laminectomy is to mill the thicker part (basically all the upper layer of cortical bone and most part of cancellous bone) first and then mill the residual part to a low thickness (0–1.2 mm), which makes the residual part quite fragile. Therefore, the residual depth of the vertebral lamina should be precisely monitored to prevent penetration of the milling tool and damage to the nerve in the spinal cord. The adaptive control of bone milling in laminectomy is dependent on recognition of the tool penetration and cutting force. The problem can be divided into two parts: judgement of the cutting state and prediction of the ADOC for inferring the cutting force. The cutting state in the bone milling of the lamina can be divided into five states, as shown in Figure 1c.

Cutting state (1): The milling tool starts to cut the bone, and the top surface of the lamina is the cortical bone. This state is relatively safe because the lamina is located far from the bottom surface. However, this state also increases the cutting force and temperature, which

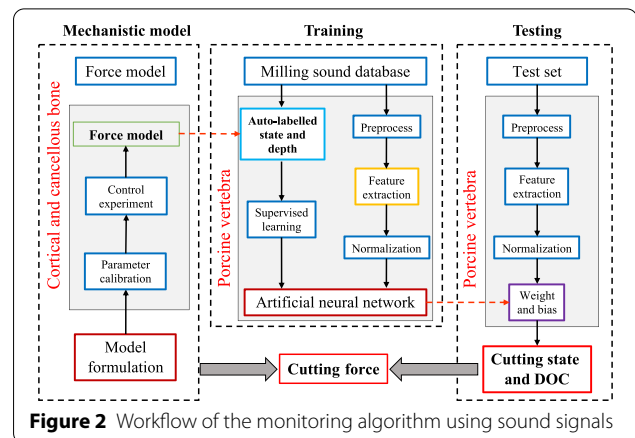
increases the risk of bone damage and tool breakage. Optimized machining parameters are preferred in this cutting state during the adaptive control of bone milling. Cutting state (2): The milling tool starts cutting the cancellous bone. The cutting force tends to reduce owing to the relatively low material strength of cancellous bone. Cutting state (3): All cutting bones are cancellous. A high feeding speed, ADOC, and low rotation speed are preferred for balancing cutting efficiency, force, and temperature in bone milling. When cutting state (4) occurs, milling is stopped, which means that the milling tool has reached the last layer. Because the bottom layer of the cortical bone varies from 3 to 10 μm , and the radius of the milling tool varies from 1.5 to 3.0 mm, penetrating the bottom surface (state 5) is easy when the cutting state reaches state (4).

After determining the cutting state, the monitoring approach predicts the ADOC of each layer (cortical bone, cancellous bone, and idle). Based on the results of the predicted ADOC and inferred cutting force, the productivity and safety of bone milling in laminectomy can be improved by integrating adaptive control algorithms [21].

3 Materials and Methods

In this study, we propose a neural network model to classify the cutting state and predict the ADOC of each layer during bone milling. Although it is difficult to estimate the ADOC by experimental video during data collection, ensuring the veracity of the training data and accuracy of the recognition model is critical. Moreover, because the vertebral lamina has an irregular shape and structure, maintaining the ADOC static in an actual bone milling experiment is difficult. First, a credible ADOC value should be estimated. Building a numerical relationship between the ADOC and force appears to be a feasible approach to accurately measure the force signal in the milling process. An overview of the workflow of this study is shown in Figure 2. The ANNs were trained using a database established using the sound signal collected during bone milling and the inferred cutting state. To improve the accuracy of state recognition, the corresponding cutting state and depth were labeled with verification of the milling force model.

Milling force modeling was performed to capture the relationship between the ADOC and the cutting state against the cutting force in the bone milling process. With an accurate numerical relationship, the cutting state and ADOC could be derived correctly using the measured cutting force, which was used to label the database. Additionally, the effect of cutting parameters (ADOC, rotation speed, and feed rate) on the milling force was investigated to provide experimental support for operation condition optimization.



3.1 Milling Force Model

A mechanistic force model is improved to estimate the cutting force in ball-end bone milling based on the early work from Lee and Lamikiz [22, 23]. This work improved the mechanistic force model with respect to the mill bit geometry and milling process parameters firstly. Then, the calibration experiments are conducted to derive the coefficients of force model. Finally, experiments with a wide range of milling conditions are used to validate the calculated results of cutting force.

The improved force model estimates the cutting force in two steps. At first, the position of the cutting tips of ball-end mill bit (Figure 3a) has been located with the discrete geometry modeling. Secondly, the cutting force is calculated by integrating on contacting area with a coordinate transformation. There are two part of length need to be calculated: the thickness of chip cut by the blade and the width of discrete element of the cutting edge. However, the ball-end milling tool is not like the normal end mill bit. It needs re-modeling with a transformed coordinate of the cutting tip on the flute. The differential force on the element of cutting edge can be calculated. At last, the cutting force on the normal coordinate can be acquired by integration.

3.1.1 Geometrical Modeling of the Ball-end Cutting Tip

Given the radius R_0 of ball-end milling tool, the positioning angle of the element Ψ can be expressed as a function of the spindle rotation angle, corresponding to the position of the cutting-edge element in the tool as shown in Figure 3b:

$$\Psi_{ij}(\theta, z) = \theta + (j - 1)\phi_p - \varphi_i(z_i), \quad (1)$$

where θ is the spindle rotation angle, φ_i is the angle gap between the i cutting edge element and the tool point, φ_0 is the total lag angle. The lag angle is a constant

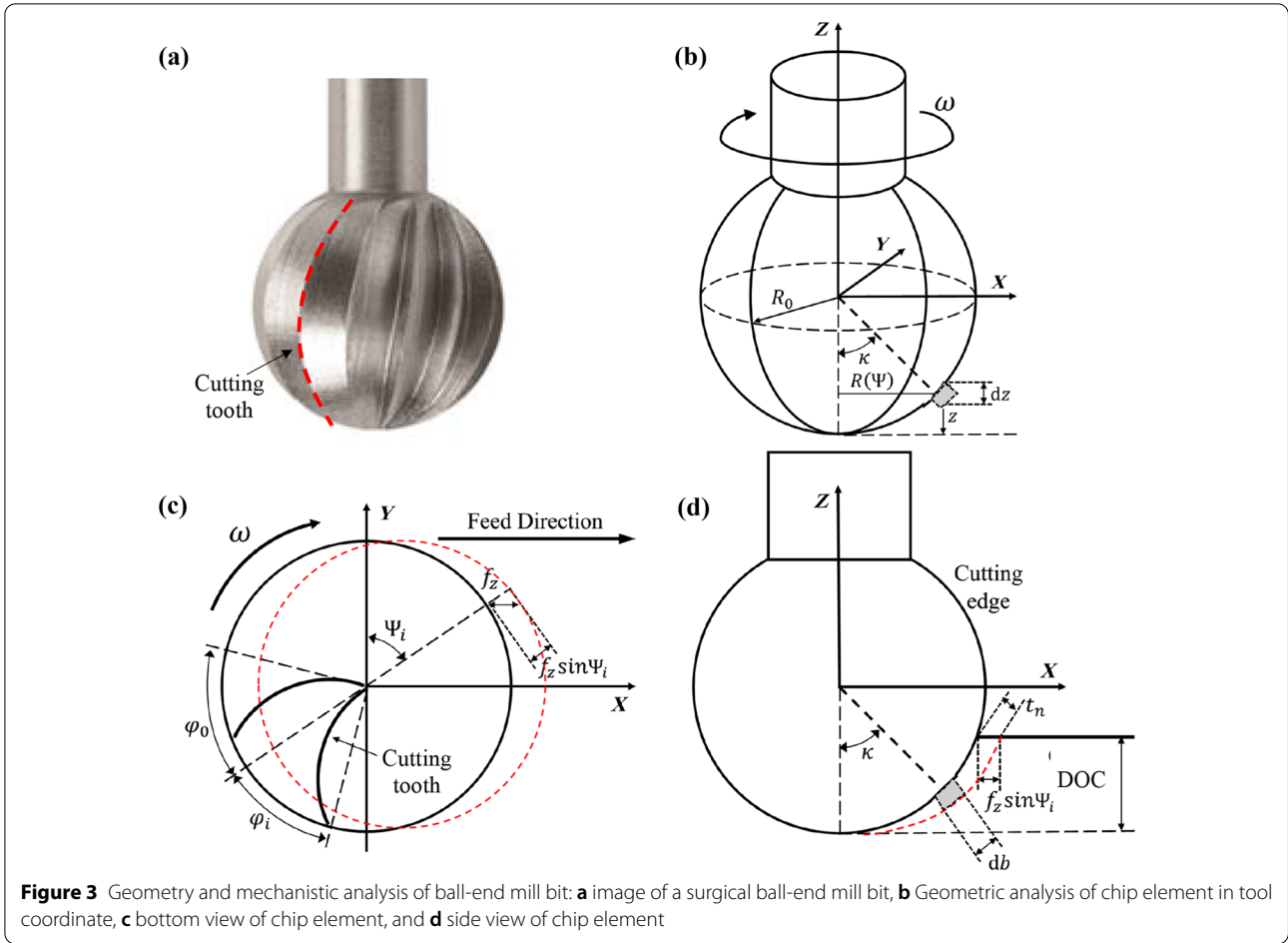


Figure 3 Geometry and mechanistic analysis of ball-end mill bit: **a** image of a surgical ball-end mill bit, **b** Geometric analysis of chip element in tool coordinate, **c** bottom view of chip element, and **d** side view of chip element

for each tool and depends on the helix angle i_0 , and the sphere radius R_0 ; φ_i is the element lag angle, which varies between zero and φ_0 . The pitch angle ϕ_p can be expressed as:

$$\phi_p = \frac{2\pi}{N_f}, \tag{2}$$

where N_f is number of flutes on the ball-end milling tool.

The point on the surface of sphere in the normal coordinate can be expressed as:

$$x_i^2 + y_i^2 + (R_0 - z_i)^2 = R_0^2. \tag{3}$$

Replacing the radius of circle at z coordinate of z_i :

$$x_i^2 + y_i^2 = R_i(z_i)^2. \tag{4}$$

As shown in Figure 3c, the z coordinate of the cutting-edge elements can be expressed by the cylindrical helix with radius of ball-end milling tool, corresponding to the nominal helix angle:

$$z_i = \frac{R_0 \varphi_i}{\tan(\varphi_0)}. \tag{5}$$

Replacing Eq. (5) into Eq. (4):

$$R_i(z_i) = R_0 \sqrt{1 - \left(\frac{z_i}{R_0} - 1\right)^2}. \tag{6}$$

Thus, the coordinates of the cutting-edge elements on x and y axis from the z coordinate and the spindle rotation angle θ , can be obtained by Eq. (6). The position of each flute in the global coordinate:

$$r_{ij}(\Psi) = R_i(\varphi_i)[\sin(\Psi)i + \cos(\Psi)j] + \frac{R_0 \varphi_i}{\tan(\varphi_0)}k. \tag{7}$$

The length of discrete element can be calculated and so as the differential form, representing the discrete element position as:

$$dS_{ij} = \|dr_{ij}\| = \sqrt{[R'_i(\varphi_i)]^2 + R_i^2(\varphi_i) + \frac{R_0^2}{\tan^2(\varphi_0)}} d\varphi, \tag{8}$$

where $R'(\varphi_i)$ is the derivative of $R(\varphi_i)$.

The uncut chip thickness as shown in Figure 3d is calculated with the angular position:

$$t_n(\Psi, \theta, \kappa) = f_z \bullet \sin(\Psi) \bullet \sin(\kappa), \tag{9}$$

where f_z is the feed per tooth; κ is the axial position angle.

On the other hand, the chip thickness of discrete element, as shown in Figure 4b, can be calculated as following:

$$db = \frac{dz}{\sin(\kappa)}. \tag{10}$$

3.1.2 Modeling of the Cutting Force

Based on the geometry modeling, the differential force on the flutes then can be calculated. The cutting force on normal coordinate can be acquired by integration of a superposition of all the forces acting on infinitesimal

segments [24, 25]. The resultant force can be divided to two parts: the shear force required to remove the chip, and the work-tool edge force. Therefore, the total force acting on the cutter can be expressed as follow:

$$\begin{bmatrix} dF_t \\ dF_r \\ dF_a \end{bmatrix} = \begin{bmatrix} K_{te} & K_{tc}t_n(\Psi, \theta, \kappa) \\ K_{re} & K_{rc}t_n(\Psi, \theta, \kappa) \\ K_{ae} & K_{ac}t_n(\Psi, \theta, \kappa) \end{bmatrix} \begin{bmatrix} dS \\ db \end{bmatrix}, \tag{11}$$

where dF_t, dF_r, dF_a (N) are the tangential, radial and axial components of cutting force, K_{tc}, K_{rc}, K_{ac} : (N/mm²) are the shear specific coefficients, K_{te}, K_{re}, K_{ae} (N/mm) are the edge specific coefficients using to adjust the ploughing force, dS (mm) is the length of each discrete elements of the cutting edge, t_n (mm) is the undeformed chip thickness, and db (mm) is the chip width in each cutting edge discrete element.

The tangential, radial and binormal cutting forces of each cutting-edge element used transformed in a unified coordinate system, the components dF_x, dF_y and dF_z as shown in following:

$$\begin{bmatrix} dF_x \\ dF_y \\ dF_z \end{bmatrix} = \begin{bmatrix} -\sin(\kappa)\sin(\Psi) & -\cos(\Psi) & -\cos(\kappa)\sin(\Psi) \\ -\sin(\kappa)\cos(\Psi) & \sin(\Psi) & -\cos(\kappa)\cos(\Psi) \\ \cos(\kappa) & 0 & \sin(\kappa) \end{bmatrix} \bullet \begin{bmatrix} dF_r \\ dF_t \\ dF_a \end{bmatrix}. \tag{12}$$

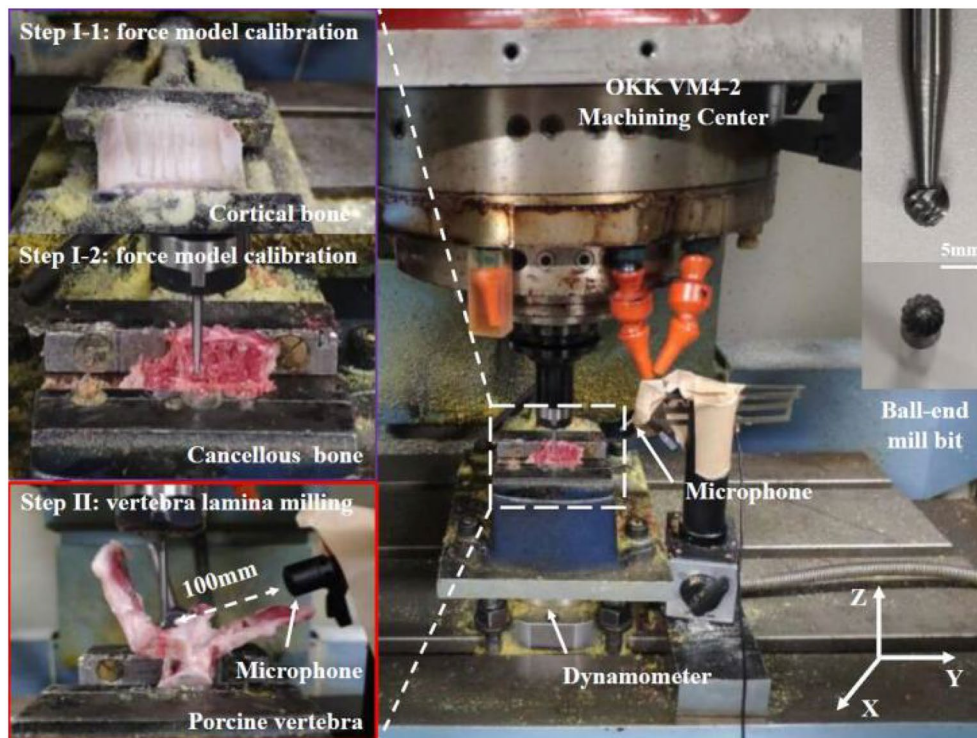


Figure 4 Experimental setup for bone milling

The resulting force can be obtained with a numerical integration along the cutting edge engaged in the machining process. The cutting force acting on the j th cutting edge could be calculated as:

$$\begin{cases} F_{xj} = \int_{z_1}^{z_2} (-\sin(\kappa)\sin(\Psi) \bullet dF_{rj} - \cos(\Psi) \bullet dF_{tj} - \cos(\kappa)\sin(\Psi) \bullet dF_{aj}) dz, \\ F_{yj} = \int_{z_1}^{z_2} (-\sin(\kappa)\cos(\Psi) \bullet dF_{rj} + \sin(\Psi) \bullet dF_{tj} - \cos(\kappa)\cos(\Psi) \bullet dF_{aj}) dz, \\ F_{zj} = \int_{z_1}^{z_2} (\cos(\kappa) \bullet dF_{rj} + \sin(\kappa) \bullet dF_{aj}) dz, \end{cases} \quad (13)$$

where z_1 and z_2 are the starting and ending z coordinate, respectively.

The milling force components F_x , F_y and F_z can be calculated on each cutting edge of the tool. The resulting force is calculated by adding the force of each of flute:

$$F = \sum_{j=1}^{N_f} F_j, \quad (14)$$

where F is the instantaneous force acting on the ball-end milling cutter.

Moreover, the integration range of every flute also depends on the spindle rotation angle θ as shown in Table 1. With the formulation of cutting force, we could estimate the cutting force along three axes with known ADOC and cutting tool parameters.

3.2 Modeling of the Cutting Force

In the bone-cutting process, the sound signal originates from bone structure breakage and bone chip extrusion. Considering that the sound signal has bone cutting information, we applied this signal to monitor the bone milling process and thus provide an adaptive control method for orthopaedic surgical robots to enhance safety. The sound generated during bone milling contains a large amount of information about the condition of the cutting state and contacting surface in the time and frequency domains. In this study, the wavelet packet transform (WPT) was chosen as the time frequency analysis method for sound signals owing to its high fixed-frequency multiresolution.

Wavelet transform is a mathematical method for solving the decomposition of nonstationary signals using

a set of orthogonal rapidly decaying wavelet function bases for signal fitting [26, 27]. The positions of the different frequency signal components in the time domain are obtained through scale and translation variates of

the wavelet function base, which means that the signal is decomposed into many frequency sub-bands and every sub-band has a series of wavelet packet coefficients. The WPT is performed using a function that decomposes the band in the high-frequency domain as follow:

$$WT_x(t, a) = \frac{1}{\sqrt{a}} \int x(u) \psi \frac{u-t}{a} du, \quad (15)$$

where wavelet $\psi \frac{u-t}{a}$ is derived by dilating and translating the wavelet basis $\psi(t)$, and $\frac{1}{\sqrt{a}}$ is a normalization factor to maintain energy conservation. The WPT with a moving window was performed to calculate the spectral features, which were used to study the frequency domain in sound processing.

To estimate the cutting state and ADOC in bone milling, the sound of the vertebral lamina milling was collected to construct the database. The processed data and labels (cutting state and ADOC) validated by the force model were then conveyed to an ANN to train the model. In this study, the Daubechies-5 wavelet was used to perform signal decomposition and 64 sets of wavelet packet coefficients on every frequency band were stacked as the input matrix of the ANN. The ANN was chosen to classify the milling state with extracted features from the milling sound, which was successfully applied in condition monitoring of manufacturing, pattern recognition, and computer vision [28]. Using the ANN, the intrinsic information contained in the milling sound signals can be clarified and the important frequency band can be screened out. The datasets in the database were divided into training (80%) and testing (20%) datasets. In our case, the ANN was trained using the training dataset.

3.3 Experimental Setup

3.3.1 Experiment for Force Model Calibration

This experiment was conducted to calibrate the cutting coefficients in the improved force model and observe the effects of cutting conditions on cortical and cancellous bone milling. The experiments were conducted on an OKK VM4-2 machining center, as shown in Figure 4. The cutting force was measured using a Kistler

Table 1 Integration limit in one pitch

θ	Integration limit	Case 1	Case 2	Case 3	Case 4
$0 < \theta < z_0 \tan(\varphi_0)/R_0$	z_1	0	0	$R_0 \cot(\varphi_0) \theta$	0
	z_2	$R_0 \cot(\varphi_0) \theta$	z_0	z_0	0
$z_0 \tan(\varphi_0)/R_0 < \theta < \varphi_0$	z_1	0	0	0	0
	z_1	z_0	z_0	0	0

Dynamometer 9272 (Kistler Inc., Switzerland), with a sampling frequency of 20 kHz. Cortical and cancellous bone samples from a fresh femur of a porcine were used as the workpiece in the force model calibration, which has biomechanical properties similar to those of human bone [29], as shown in Figure 4 (Step I-1, Step I-2). The bone sample was placed vertically to the rotating spindle to ensure that the ADOC was stable and unchanged during the entire milling process. The detailed experimental conditions are presented in Table 2.

The sound of milling cortical and cancellous bone was collected to understand the cutting characteristics of different bone milling techniques. In addition, the depth of cut, rotation speed, and feed rate were considered, and appropriate milling values were chosen in the construction of the database.

3.3.2 Experiment for Monitoring Test of Vertebra Lamina Milling

The experimental setup used to validate the monitoring method is shown in Figure 4 (Step II). The milling tool and operational environment were the same as those in the previous experiments on the flat bone specimen. The cutting force and sound signals were collected simultaneously. Fresh porcine vertebrae were chosen for use as the bone specimen in our study. In the continuous experimental procedures of vertebra milling, the ADOCs were controlled as 0.5 and 1.0 mm to bring milling conditions closer to the real laminectomy. The sound signals were measured by a wired commercial microphone (RS Inc. Japan) with a sampling rate of 48000 Hz in all experiments and transported to PC for further analysis. Each of the sound data sample was processed with differential amplification, bandwidth limitation (450 to 24000 Hz) and WPT to extract the amplitude information of sound signals. The detailed experimental conditions are listed in Table 3

Table 2 Parameters of the experiment for force model calibration

Items	Parameters
Test bone	Cortical and cancellous bone (Porcine femur)
Rotation speed(r/min)	1000, 3000, 5000
Tool diameter(mm)	5
Tool flute number	12
Tool helix angle(°)	30
Feed rate	1.5, 2, 2.5
ADOC(mm)	0.25, 0.5, 0.75, 1.0, 1.25

Table 3 Parameters of vertebra milling experiment.

Items	Parameters
Test bone	Porcine vertebra
Rotation speed(r/min)	1000, 3000, 5000
Feed rate(mm/s)	1.5, 2, 2.5
ADOC(mm)	0.5, 1.0

4 Results and Discussion

4.1 Force Model Calibration and Coefficient Calculation

The milling forces on the cortical and cancellous bones under the same milling conditions are shown in Figure 5. With the local features of the force and the procedures we set in the experiments, the entire milling process can be separated into four phases: penetration, stable cutting, evacuation, and non-cutting phases. A significantly

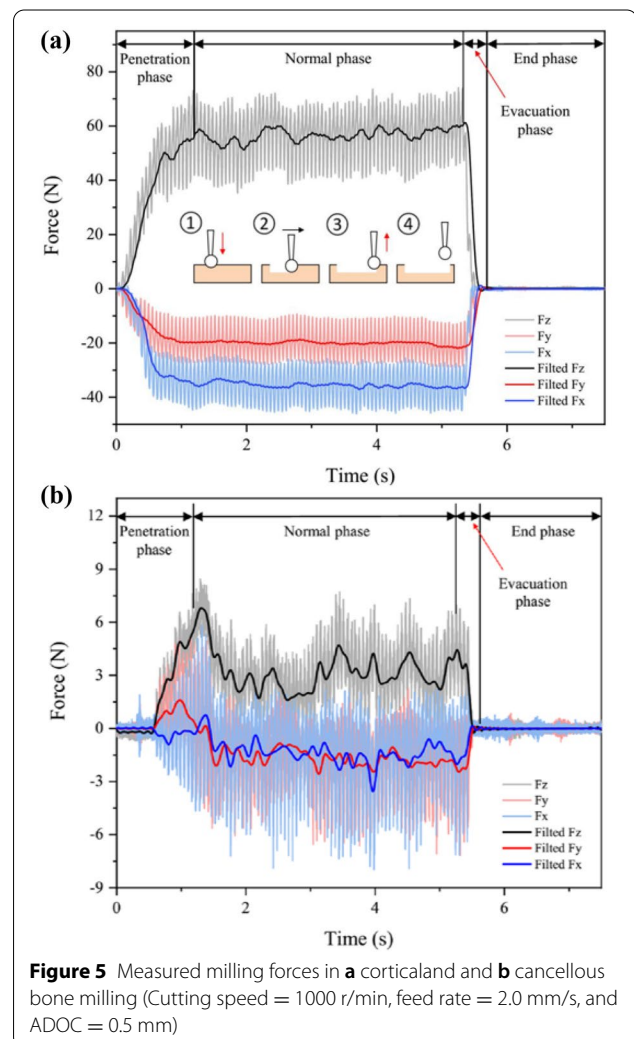


Figure 5 Measured milling forces in **a** cortical and **b** cancellous bone milling (Cutting speed = 1000 r/min, feed rate = 2.0 mm/s, and ADOC = 0.5 mm)

lower cutting force can be observed in cancellous bone milling than in cortical bone milling. A sixth-order low-pass Butterworth filter was selected to smooth the curve of the cutting force with a 200 Hz cut-off frequency. The calibrating value of the cutting force under specific processing conditions was calculated using the average value of the filtered cutting force in the stable cutting phase and optimized by the particle swarm optimization algorithm [30]. Three sets of experimental data (depth = 0.5, 0.75, 1.25 mm) were used to optimize the coefficients, and the remaining two sets (depth = 0.25, 1.0 mm) were used to evaluate the accuracy of the force model. After 100000 iterations, the fitness function reached a score of 0.1 and the results of the optimized coefficient are listed in Table 4.

Once the coefficients of the force model are obtained, the cutting force of bone milling can be predicted under various ADOC conditions. Figure 6 presents example results of the measured and calculated forces on the cortical and cancellous bone, respectively. A similar variation tendency was found between the experimental data and predicted results. Compared with the results of predicted and experimental cutting force in the depths of cut of 0.25 mm and 1.0 mm, the developed force model predicted the cutting force with a maximum deviation of 6.38% under unknown milling conditions. The force model also predicted an abrupt decrease in the set of 0.25 mm. Because the cutting performance was poor at the top of the ball-end mill bit, the material removal rate could not effectively increase with increasing ADOC.

Because the force model could predict the milling force under a specific milling condition, the effect of a wide range of milling parameters on the cortical bone (predominant in cutting force components) was investigated to find an optimal condition for vertebral lamina milling, as shown in Figure 7. Based on the results, a milling condition (cutting speed = 3000 r/min and feed rate=2.0 mm/s) was adopted for the subsequent experiments.

Because the force model can fit the actual cutting force components along the three axes, it can be used to auto-label the cutting state and ADOC in complex bone milling. The force corresponding to specific ADOC and the

Table 4 Coefficient of the force model

Bone layer	Edge coefficients		Shear coefficients	
Cortical bone	K_{te}	3.8269	K_{tc}	5973.4+1620.5z
	K_{re}	-5.2733	K_{rc}	-28312.5-1693.1z
	K_{ae}	12.9675	K_{ac}	-41296.3+12595.1z
Cancellous bone	K_{te}	0.3692	K_{tc}	370.8-532.3z
	K_{re}	-0.5615	K_{rc}	-105.8-591.4z
	K_{ae}	0.9238	K_{ac}	-2941.1+4088.2z

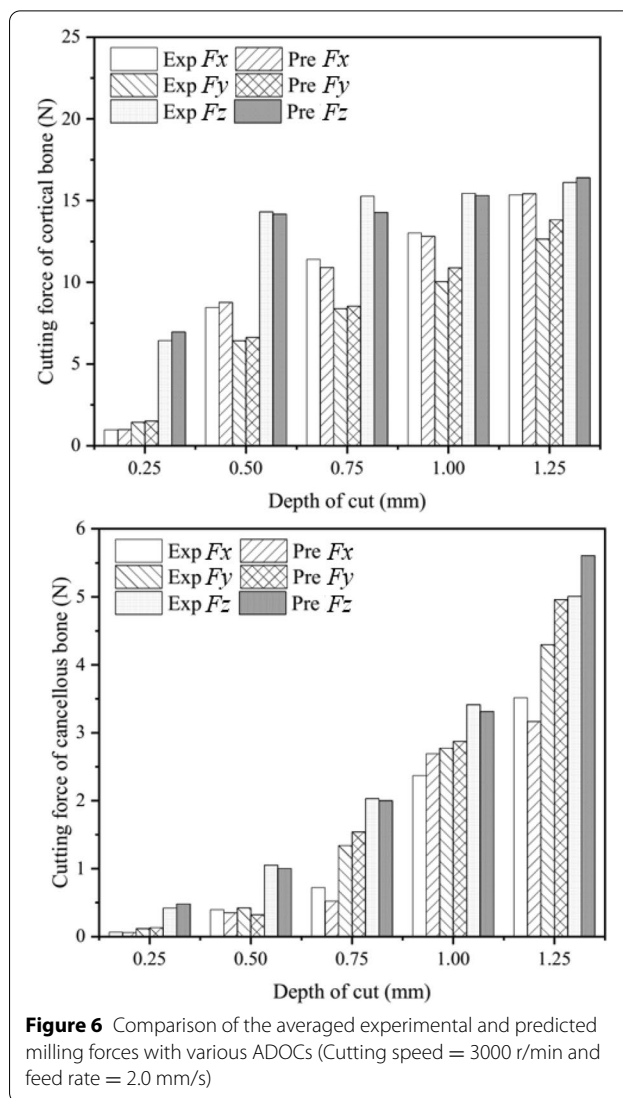


Figure 6 Comparison of the averaged experimental and predicted milling forces with various ADOCs (Cutting speed = 3000 r/min and feed rate = 2.0 mm/s)

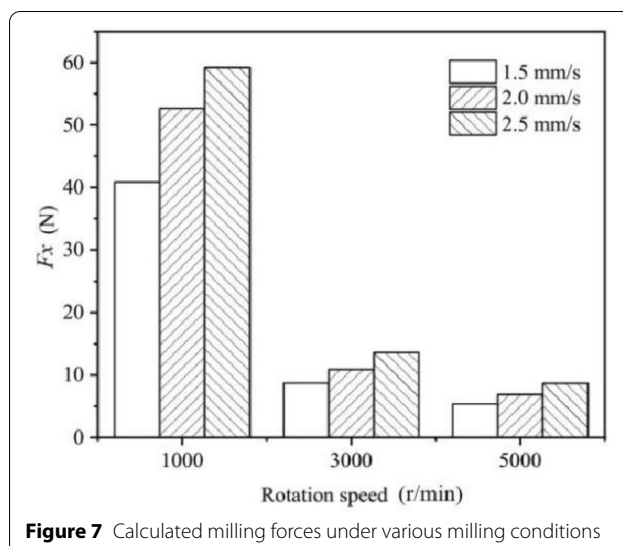
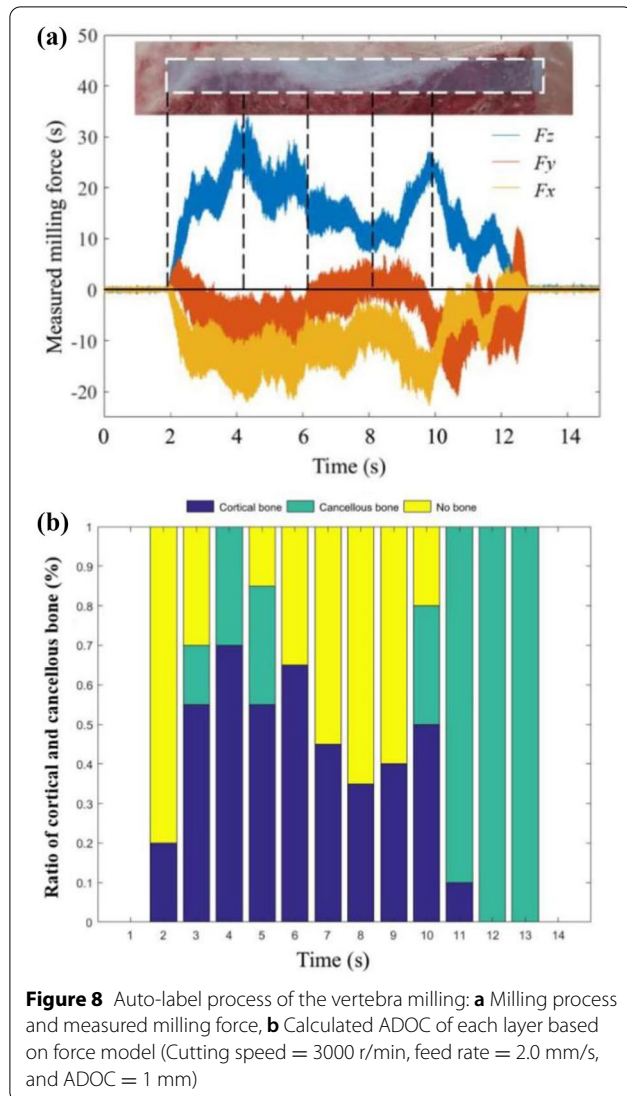


Figure 7 Calculated milling forces under various milling conditions

ratio of cortical and cancellous bone can be calculated based on the proposed milling force model. As the milling force of cortical bone is much larger than cancellous bone with same ADOC, the relationship between the milling force and cortical-to-cancellous ratio is monotone increasing, avoiding yielding various possibilities with a given cortical-to-cancellous ratio. Moreover, the model can be used to monitor the cutting force when milling irregular surfaces under certain milling conditions, instead of using a force sensor.

4.2 Cutting State and ADOC Monitoring Using Sound Signal

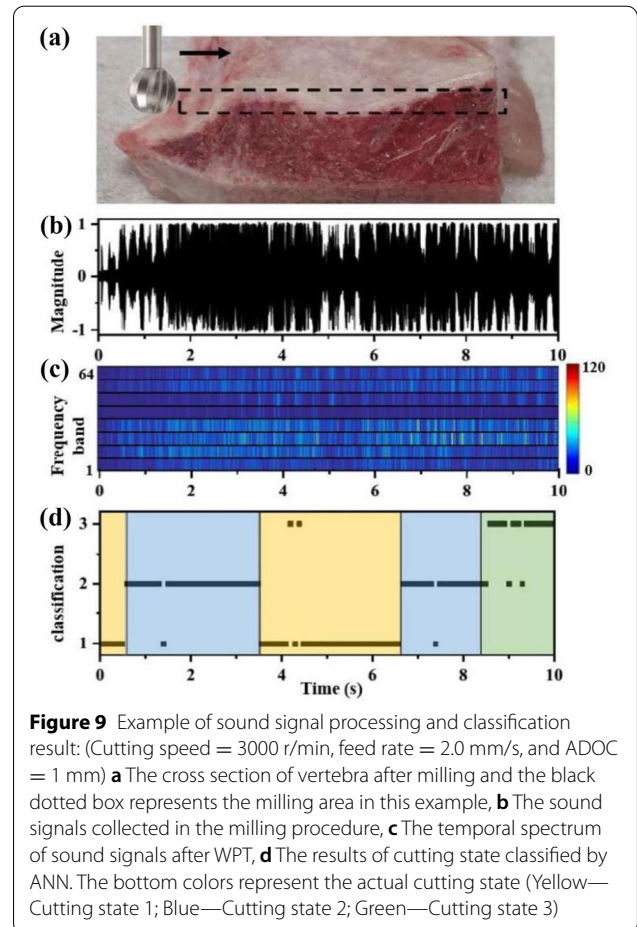
An auto-label result of the cutting state and ADOC in vertebral lamina milling is shown in Figure 8. The measured force was used to validate the proposed ADOC using the milling force model. In sound signal processing,

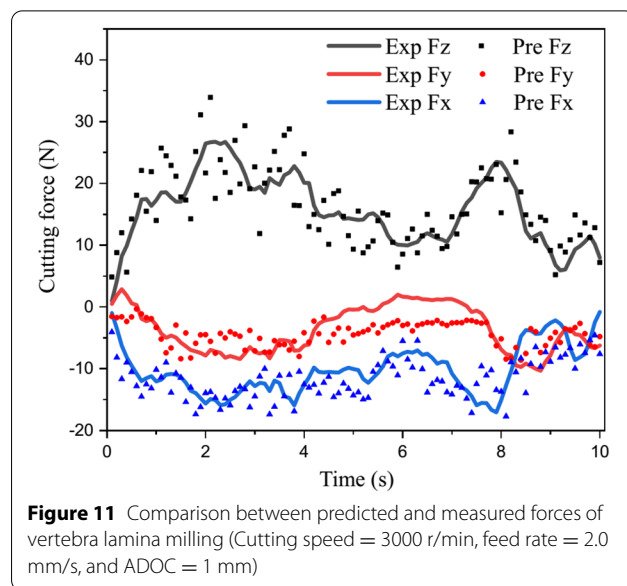
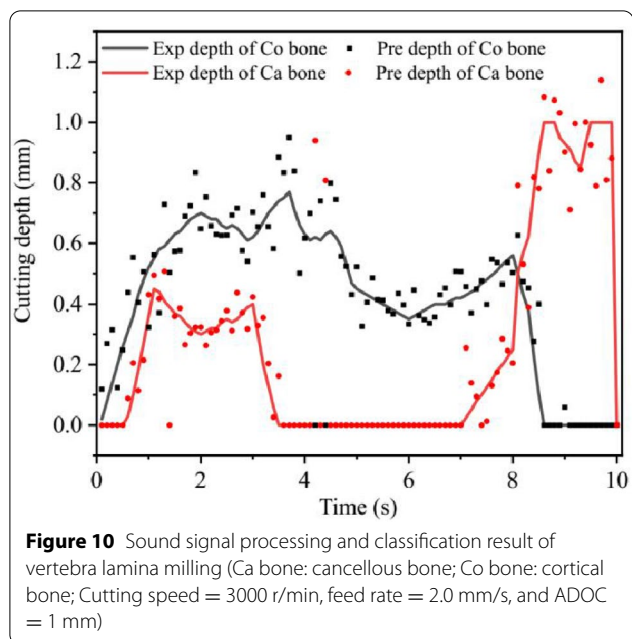


the data flow was divided into 0.1 s packages. Similarly, the cutting force was also averaged with a time length of 0.1 s to calculate the ADOC, as shown in Figure 8b.

The typical milling region and corresponding sound samples in the milling of the vertebral lamina (length of 10 s) are shown in Figure 9a and b, respectively. The top-layer milling process was chosen to show the differences between various cutting states and ADOCs on the signal and processed WPT coefficients. The actual values of the cutting state and ADOC, as shown in Figures 9d and 8c, represent the three cutting states and the changes in the ADOC with time.

The processed WPT temporal spectrum is shown in Figure 9c. The differences in cutting states are evident and are expressed in terms of the magnitude of spectral density and wavelet energy. The wavelet energy was larger when cutting cancellous bone than cortical bone in more WPT high-frequency sub-bands because cancellous bone is a spongy bone tissue with dense porous spaces. The WPT energy ratios of all the sub-bands were chosen as features of the ANN because of their excellent ability to process redundant information. Additionally,





the features in the wavelet domain were used to consider the other sound features to effectively regress the ADOC. The cutting state and ADOC results are shown in Figures 9d and 10. Seven classification errors occurred in one milling process (length of 100 time packages) during the unsteady and changing phases of the cutting state.

After estimating the cutting state, the ANN can predict the possible depth of each bone layer based on the results of the cutting state. The predicted ADOCs are mostly on par with the supposed ADOCs labeled by the force model and the measured milling force signals. The ANN performed well when the bone milling tool made contact with cancellous bone. One disadvantage of this approach is that the ANN cannot correctly predict the ADOC if a classification mistake occurs. One disadvantage of this approach is that the ANN could not predict ADOC correctly if a classification mistake happened.

To examine the performance of milling force monitoring, the calculated force values based on the predicted ADOC and the actual milling force measured in the experiment were compared, as shown in Figure 11. The milling force on the *x*-axis exhibited a better fitting relationship because the labeled ADOC was mainly calibrated by the measured force.

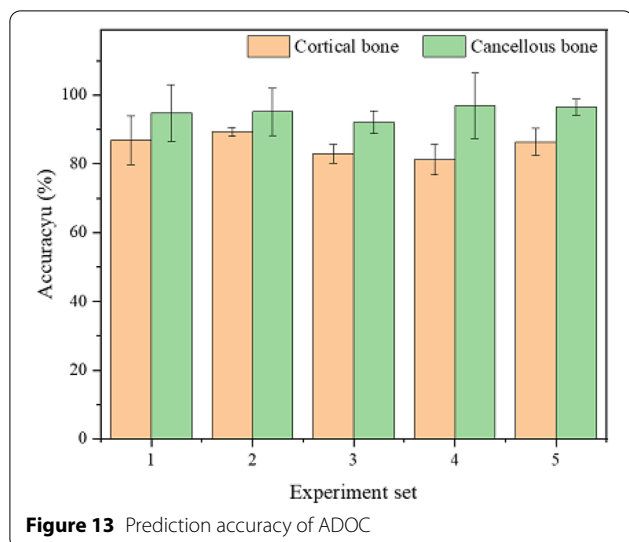
The confusion matrix of the prediction result used to evaluate the performance of the trained ANN model is shown in Figure 12. This test set contained 750 data packages, of which 723 packages were tested correctly. The classification mistakes occurred in distinguishing between cutting state 2 and 4, which are both related to cortical and cancellous bone. This mistake is resulted

from that sound signal features of two cutting states are highly correlated in the frequency domains. Erroneously identifying a true cutting state (4) as a mistake is perilous, as it indicates that a dangerous penetration had occurred and that the system had not noticed it. The high accuracy resulted from the accurate classification of cancellous bone milling, whose WPT features were distinct from those being recognized.

The accuracy of the cross-validation of ADOC prediction is shown in Figure 13. As the data of all sets were collected from different vertebrae, it was concluded that our model has an excellent generalization of bone properties. This also indicates the possible clinical application of the model to actual surgery where patient bone information does not have to be collected in advance. The accuracy of predicting the ADOC of cancellous bone is higher than that of cortical bone, which results from the

		Predicted state					
		State 1	State 2	State 3	State 4	Idle	
True state	State 1	9.33%	0.27%	0.00%	0.00%	0.13%	95.89%
	State 2	0.13%	7.33%	0.00%	0.27%	0.00%	94.83%
	State 3	0.00%	0.13%	45.47%	0.40%	0.67%	97.43%
	State 4	0.40%	0.27%	0.13%	10.53%	0.13%	91.86%
	Idle	0.13%	0.40%	0.00%	0.13%	23.73%	97.27%
		93.33%	87.30%	99.71%	92.94%	96.22%	96.40%

Figure 12 Confusion matrix to classify cutting states



depth of most cutting states (3) being stable with considerably more training data.

Based on the experimental results, a strategy for detecting bone milling penetration was proposed. It is safe to detect cutting states (1) and (2). When state (3) is detected, the alarm system is activated. Following the prediction of cutting state (4) and depth of cut, bone milling is supposed to cease when the depth of the cortical bone is more than 0.3 mm. Although the residual thickness of the lamina is more than 0.7 mm, the surgeon can easily remove it. This proves that detection of tool penetration using sound signal in real robot-assisted surgical environments can be employed.

Consequently, the mathematical model-based method proposed here follows the steps can be employed to monitor the bone milling procedure: (1) Calculate the milling forces of all axes to get the representation of milling procedure; (2) Extract the ADOC of different bone layers from each cutting states corresponding to different milling forces; (3) Decompose the sound signal by using WPT and predict the milling force and cutting state using ANN.

The limitation of this study is the proposed model cannot be adapted to deal with variant feed orientation at a tilted angle, which is a common scenario in hand-actuated surgery [4]. Developing a milling force model at a tilted angle is a challenging research issue for further work.

5 Conclusions

In this study, a method for monitoring the cutting state and force was proposed to provide a safe surgical environment for bone milling. The proposed monitoring algorithm is based on an ANN and a sound signal. To

establish a well-labeled database, an improved force model was developed to predict the cutting force based on ADOC in ball-end bone milling. The calculated milling forces were in good agreement with both the magnitude of the experimental results and the variance tendency. In the process of collecting bone milling sounds, the features of the sound signal were extracted from the temporal, spectral, and wavelet domains. The trained model could detect the cutting state and penetration depth of bone milling. The results revealed a 3.6% error of state recognition and a 7%–13% error of depth prediction in the bone milling scenarios.

Acknowledgements

Not applicable.

Author contributions

ZY: writing—original draft, methodology, formal analysis, investigation; LS: writing—review & editing, conceptualization, supervision, funding acquisition; NS: writing—review & editing, resources, supervision. All authors read and approved the final manuscript.

Authors' Information

Zhenzhi Ying, born in 1995, is currently a PhD candidate at *Manufacturing Laboratory, Department of Mechanical Engineering, The University of Tokyo, Japan*. He received his Bachelor degree from *Zhejiang University, China*, in 2018 and Master degree from *The University of Tokyo, Japan*, in 2020. His research interests include human-machine interface and biomanufacturing. Tel: +81-03-5841-6336.

Liming Shu, born in 1990, is currently a Lecturer in bio-design and manufacturing at *The University of Tokyo, Japan*. He received his PhD degree in Mechanical Engineering in *The University of Tokyo, Japan*, in 2018. His current research interests include human neuro-biomechanics modelling and biomanufacturing in facing for precision medicine.

Naohiko Sugita, born in 1970, is currently a Professor at *Manufacturing Laboratory, Department of Mechanical Engineering, The University of Tokyo, Japan*.

Funding

Supported by the Open Research Fund of State Key Laboratory of Digital Manufacturing Equipment and Technology, Huazhong University of Science and Technology (Grant No. DMETKF2020004).

Competing Interests

The authors declare no competing financial interests.

Author Details

¹Department of Mechanical Engineering, School of Engineering, The University of Tokyo, 7-3-1 Hongo, Bunkyo-ku, Tokyo 1138656, Japan. ²Research into Artifacts Center for Engineering, School of Engineering, The University of Tokyo, 7-3-1 Hongo, Bunkyo-ku, Tokyo 1138656, Japan.

Received: 1 June 2021 Revised: 23 April 2022 Accepted: 29 April 2022

Published online: 31 May 2022

References

- [1] Z Chen, Y Zhang, C Wang, et al. Understanding the cutting mechanisms of composite structured soft tissues. *Int. J. Mach. Tools Manuf.*, 2021, 161: 103685.
- [2] J A Robles-Linares, D Axinte, Z Liao, et al. Machining-induced thermal damage in cortical bone: Necrosis and micro-mechanical integrity. *Mater. Des.*, 2021, 197: 109215.
- [3] Z Jiang, X Qi, Y Sun, et al. Cutting depth monitoring based on milling force for robot-assisted laminectomy. *IEEE Trans. Autom. Sci. Eng.*, 2020, 17(1): 2–14.

- [4] Z Ying, L Shu, N Sugita. Autonomous penetration perception for bone cutting during laminectomy. *2020 IEEE RAS/EMBS International Conference for Biomedical Robotics and Biomechatronics*, 2020, 21(1): 1–9.
- [5] N Sugita, T Nakano, T Kato, et al. Tool path generator for bone machining in minimally invasive orthopedic surgery. *IEEE/ASME Trans. Mechatronics*, 2010, 15(3): 471–479.
- [6] D Hill, T Williamson, C Y Lai, et al. Robots and tools for remodeling bone. *IEEE Rev. Biomed. Eng.*, 2020, 13: 184–198.
- [7] Q Li, Z Du, H Yu. Grinding trajectory generator in robot-assisted laminectomy surgery. *Int. J. Comput. Assist. Radiol. Surg.*, 2021, 16(3): 485–494.
- [8] Liming Shua, Shihao Lia, Makoto Terashima, et al. A novel self-centring drill bit design for low-trauma bone drilling. *Int. J. Mach. Tools Manuf.*, 2020, 154: 103568.
- [9] Y Sun, L Wang, Z Jiang, et al. State recognition of decompressive laminectomy with multiple information in robot-assisted surgery. *Artif. Intell. Med.*, 2020, 102: 101763.
- [10] K I A lateef Al-Abdullah, H Abdi, C P Lim, et al. Force and temperature modelling of bone milling using artificial neural networks. *Meas. J. Int. Meas. Confed.*, 2017, 116: 25–37.
- [11] N Crawford, N Johnson, N Theodore. Ensuring navigation integrity using robotics in spine surgery. *J. Robot. Surg.*, 2020, 14(1): 177–183.
- [12] Z Liao, D A Axinte. On monitoring chip formation, penetration depth and cutting malfunctions in bone micro-drilling via acoustic emission. *J. Mater. Process. Technol.*, 2016, 229: 82–93.
- [13] D Wu, C Jennings, J Terpenney, et al. A comparative study on machine learning algorithms for smart manufacturing: tool wear prediction using random forests. *J. Manuf. Sci. Eng.*, 2017, 139: 7.
- [14] D M D'Addona, A M M S Ullah, D Matarazzo. Tool-wear prediction and pattern-recognition using artificial neural network and DNA-based computing. *J. Intell. Manuf.*, 2017, 28(6): 1285–1301.
- [15] Z Ying, L Shu, T Kizaki, et al. Hybrid approach for onsite monitoring and anomaly detection of cutting tool life. *Procedia CIRP*, 2021, 104: 1541–1546.
- [16] Y Dai, Y Xue, J Zhang, et al. Biologically-inspired auditory perception during robotic bone milling. *2017 IEEE Int. Conf. Robot. Autom.*, 2017: 1112–1116.
- [17] F Guan, Y Sun, X Qi, et al. State recognition of bone drilling based on acoustic emission in pedicle screw operation. *Sensors*, 2018, 18: 5.
- [18] Z Deng, Haiyang Jin, Ying Hu, et al. Fuzzy force control and state detection in vertebral lamina milling. *Mechatronics*, 2016, 35: 1–10.
- [19] S Y Nottestad, J J Baumel, D B Kimmel, et al. The proportion of trabecular bone in human vertebrae. *J. Bone Miner. Res.*, 1987, 2(3): 221–229.
- [20] R Xu, A Burgar, N A Ebraheim, et al. The quantitative anatomy of the laminae of the spine. *Spine*, 1999, 24(2): 107–113.
- [21] N Sugita, F Genma, Y Nakajima, et al. Toolpath optimization for a milling robot of minimally invasive orthopedic surgery. *Proceedings - IEEE International Conference on Robotics and Automation*, 2007: 2273–2278.
- [22] A Lamikiz, L N L De Lacalle, J A Sánchez, et al. Cutting force estimation in sculptured surface milling. *Int. J. Mach. Tools Manuf.*, 2004, 44(14): 1511–1526.
- [23] A Lamikiz, L N Lopez De Lacalle, J A Sanchez, et al. Calculation of the specific cutting coefficients and geometrical aspects in sculptured surface machining. *Mach. Sci. Technol.*, 2005, 9(3): 411–436.
- [24] K. Denis et al., Influence of bone milling parameters on the temperature rise, milling forces and surface flatness in view of robot-assisted total knee arthroplasty. *International Congress Series*, 2001, 1230: 300–306.
- [25] Z Jiang, X Qi, Y Sun, et al. Cutting depth monitoring based on milling force for robot-assisted laminectomy. *IEEE Trans. Autom. Sci. Eng.*, 2019: 1–13.
- [26] C Sun, Chi Zhang, X Chen, et al. Deep residual network with hybrid dilated convolution for gearbox fault diagnosis. *Proceedings of the International Symposium on Flexible Automation*, 2018: 318–324.
- [27] M Zhao, M Kang, B Tang, et al. Deep residual networks with dynamically weighted wavelet coefficients for fault diagnosis of planetary gearboxes. *IEEE Trans. Ind. Electron.*, 2018, 65(5): 4290–4300.
- [28] S Elanayar, Y C Shin. Radial basis function neural network for approximation and estimation of nonlinear stochastic dynamic systems. *IEEE Trans. Neural Networks*, 1994, 5(4): 594–603.
- [29] J Aerssens, S Boonen, G Lowet, et al. Interspecies differences in bone composition, density, and quality: Potential implications for in vivo bone research. *Endocrinology*, 1998, 139(2): 663–670.
- [30] M Clerc. Particle swarm optimization, part. *Swarm Optim.*, 2010: 1942–1948.

Submit your manuscript to a SpringerOpen[®] journal and benefit from:

- Convenient online submission
- Rigorous peer review
- Open access: articles freely available online
- High visibility within the field
- Retaining the copyright to your article

Submit your next manuscript at ► [springeropen.com](https://www.springeropen.com)
